CHALMERS
UNIVERSITY OF TECHNOLOGY

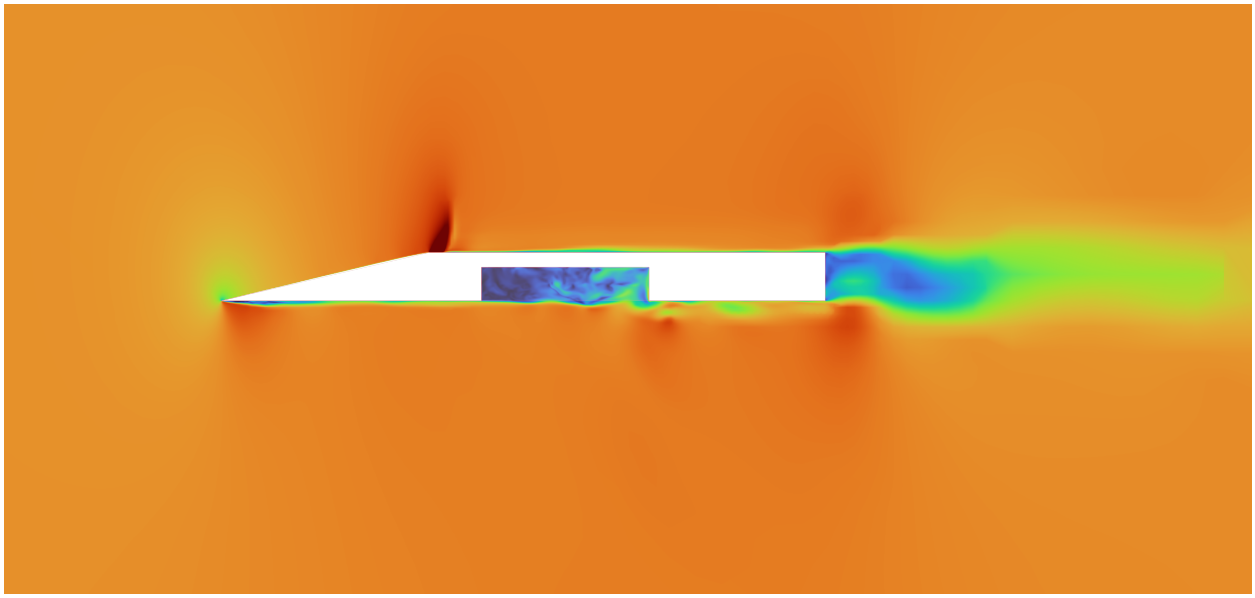

A Numerical Study on Aero-Vibro Noise of a Transonic Cavity Flow

A Report in TRA270 Engineering Fluid-Structure Interaction: Technologies and Practices

OLIVER KADI
MARTIN MAIERHOFER
BERKEN SERBÜLENT
OSKAR STÅHLBOM

Department of Mechanics and Maritime Sciences
CHALMERS UNIVERSITY OF TECHNOLOGY
Gothenburg, Sweden 2025

Project Course TRA270 2024

A Numerical Study on Aero-Vibro Noise of a Transonic Cavity Flow

A Report in TRA270 Engineering Fluid-Structure Interaction: Technologies and Practices

OLIVER KADI
MARTIN MAIERHOFER
BERKEN SERBÜLENT
OSKAR STÅHLBOM

CHALMERS
UNIVERSITY OF TECHNOLOGY

Department of Mechanics and Maritime Sciences
Division of Fluid Dynamics

Chalmers University of Technology
University of Gothenburg

Gothenburg, Sweden 2025

A Numerical Study on Aero-Vibro Noise of a Transonic Cavity Flow
A Report in TRA270 Engineering Fluid-Structure Interaction: Technologies and Practices

OLIVER KADI

MARTIN MAIERHOFER

BERKEN SERBÜLENT

OSKAR STÅHLBOM

Examiner: Hua-Dong Yao, Department of Mechanics and Maritime Sciences

Report TRA270 2024 Department of Mechanics and Maritime Sciences
Division of Fluid Dynamics
Chalmers University of Technology
SE-412 96 Gothenburg
Telephone +46 31 772 1000

Coover: Visualization of the flow around the M219 geometry, showing a cut plane colored by Mach number. The color bar has been excluded for aesthetic clarity.

Typeset in LaTeX
Gothenburg, Sweden 2025

Contribution Report

Report Writing overview

Table 0.1: Table of chapters and their **main author** and co-authors. All chapters have been edited and proofread by all.

Chapter	**Author**
Abstract	**Oliver**
Introduction	Martin, **Oliver**
1.1 Background	**Oliver**
1.2 Scope	**Oliver**
1.3 Delimination	**Oliver**
Theory	**Oskar**, **Oliver**
Methods	**Berken**, **Oskar**, **Martin**
3.1 Model Setup and Mesh	**Berken**, **Oskar**, **Martin**
3.2 Fluid Setup	**Berken**, **Martin**
3.3 Solid Setup	**Oskar**, **Martin**
3.4 Fluid-Structure-Interaction Setup	**Martin**
3.5 Aeroacoustics	**Berken**, **Oskar**
Results	**Berken**, **Oskar**
4.1 Mesh	**Berken**, **Oskar**
4.2 The URANS approach	**Berken**, **Oskar**
4.3 The IDDES approach	**Berken**, **Oskar**
Discussions	**Berken**, **Oliver**, Oskar
Conclusion	**Oliver**

Simulation Contributions

Table 0.2: Division of labor in gathering simulation results for key analyses.

Simulation Task	**Main Contributor**
Computational Fluid Dynamics with FSI	**Berken**
Eigen Frequency Analysis Results	**Oskar**
Post-processing	**Berken**

A Numerical Study on Aero-Vibro Noise of a Transonic Cavity Flow
A Report in TRA270 Engineering Fluid-Structure Interaction: Technologies and Practices
OLIVER KADI, MARTIN MAIERHOFER, BERKEN SERBÜLENT, OSKAR STÅHLBOM
Department of Mechanics and Maritime Sciences
Division of Fluid Dynamics
Chalmers University of Technology

Abstract

This report is part of a project course TRA270 Engineering Fluid-Structure Interactions (FSI) that numerically investigates the Aero-Vibro noise of a transonic cavity. Inspired by previous works this project sets up a numerical solution for this case study. Therefore, the scope of the investigation is limited by several factors, primarily the availability of computational resources and time to the nature of this project being a course. After understanding the fundamentals of FSI, the M219 cavity is meshed using an unstructured trimmed cell mesher with prism layer for the fluid domain. The solid domain was discretized and coupled in STAR-CCM+ using a quadrilateral mesh. The solid-fluid two-way coupled simulation was completed in STAR-CCM+, with mostly standardized solver settings for ideal coupled flows and non-elastic deformation. Sparlart-Allmaras (SA) turbulence model is used because it provides a smaller mesh with faster computing time and provides results comparable to the original report. In addition to investigating a hybrid RANS-LES method, an unsteady RANS (URANS) method was investigated. A comparison between the methods is presented where the change is observed to be substantial with a clear and decisive advantage towards the hybrid method.

Keywords: Fluid-Structure Interactions (FSI), Transonic, STAR-CCM+, Cavity flow, RANS, LES, IDDES, M219.

Acknowledgements

We extend our deepest gratitude to Hua-Dong Yao for organizing the course *TRA270 (2024) Engineering Fluid-Structure Interaction: Technologies and Practices*. His support and dedication in addressing questions related to Siemens Simcenter STAR-CCM+ and other topics have been invaluable.
We also wish to express our heartfelt thanks to the guest lecturers Heng Zhu, Jesper Oppelstrup, Arion Pons, Laura Marmon Giovannetti, and Lukas Schickhofer. Their engaging sessions and expertise have been instrumental in sparking our interest in the multifaceted field of fluid-structure interaction.

O. Kadi, M. Maierhofer, B. Serbülent, O. Ståhlbom, Gothenburg, January 2025

Contents

Nomenclature

Abbreviations

APE Acoustic Pertubation Equations
BC Boundary Conditions
CAA Computational Aeroacoustics
CFD Computational Fluid Dynamics
CSM Computational Solid Mechanics
DES Detached Eddy Simulation
FE Finite Element
FSI Fluid Structure Interaction
FW-H Ffwocks William-Hawking Equations
IDDES Improved Delayed Detached Eddy Simulations
LEE Linear Euler Equations
NAISS The National Academic Infrastructure for Supercomputing in Sweden
OASPL Overall Sound Pressure Level
RANS Reynolds-averaged Navier-Stokes
RAT Ram Air Turbine
SA Spalart-Allmaras
SPL Sound Pressure Level
STAR-CCM+ Siemens Simcenter STAR-CCM+
SUPR Swedish User and Project Repository
URANS Unsteady Reynolds Avaraged Navier-Stokes

Variables

$\overline{v}$ Mean flow velocity
c_p Specific Heat
k Thermal Conductivity
M Molecular Weight
Pr Prandtl Number
v' Fluctuating velocity
y^+ Non-dimensional wall distance
v Velocity

List of Figures

List of Tables

1
Introduction

Fluid-structure interactions (FSI) are an interesting and growing area of investigation. Many applications benefit from understanding the complexities of coupling solvers that investigate the interactions between fluid dynamics and structural mechanics. With ever-evolving construction methods, investigating these problems will reveal dimensioning criteria that have not previously been studied as closely. A variety of cases can be studied but for this project, this research group has decided to investigate cavity flows in a transonic regime.

1.1 Background

Cavity flows are present in several aerospace applications, civil and military alike. In civil aerospace, this can constitute of the landing gear bay or the ram air turbine (RAT) opening. Whereas for military applications this can constitute weapon bays, cargo openings, or any other necessary cavity. Cavity flows are unsteady and will result in pressure fluctuations generating noise [1]. Some differences can be observed in the depth of the cavity itself, in the case of shallow cavities, broadband noise dominates, and in the case of deeper cavities tonal components dominate, these tonal components can be referred to as Rossiter modes [2]. These pressure fluctuations can be energetic and have a large effect on aerodynamics, noise both internal and external, and in many cases structural integrity. Vibrations are commonly observed in these cases and can cause instabilities, failures, acoustic fatigue or even cause other components to be exposed to this vibration.

Transonic cavity flows can be classified as high Reynolds number flows. A multitude of studies have been conducted, numerical and experimental [3, 4]. Different turbulence regimes have been discussed by a multitude of previous studies. The consensus from such studies is that high Reynolds cavity flows are challenging to resolve.

1.2 Scope

The scope of this project is to investigate similar conditions to the article published by S. Nilsson et al [5]. The previous investigations into Unsteady Reynolds-Averaged Navier-Stokes (URANS) solution reported less accurate results but will be used as a benchmark in this report [6, 7]. Large-eddy simulations (LES) provide exceptional

results but are consuming. A good middle ground is hybrid RANS-LES methods, which seem to agree with experimental data as seen in [3, 8–10]. In addition, correct turbulence resolution is highly important; therefore, using a hybrid RANS-LES has been successfully used in many studies [11]. Elastic cavity walls have been examined but are complex and will be neglected in this project. However, it is important to note that the works of Łojek et al. [12] show the possible integration, at least for low Reynolds numbers.

In this project, the M219 cavity is examined and integrated into STAR-CCM+. The results are then compared to S. Nilsson et al [5] results as well as the experimental data by Henshaw [13] and the LES data by Lerchevêque et al. [14]. Sound pressure levels (SPL) will be used to understand the tones emitted by the cavity during fluid-structure interactions. Spectral proper orthogonal decomposition (SPOD) is used to understand the wall pressure fluctuations. These methods are then used to evaluate the results with LES data.

1.3 Delimitation

Due to the nature of this project being a course, cluster computing resources are limited. In combination with the time assigned for this course being a single study period, deep investigations into optimal solvers and advanced settings will be disregarded. Instead, this report will focus on the quality of the data obtained within the mentioned constraints. The project will therefore only investigate a rigid body cavity using the Spalart-Allmaras (SA) turbulence modelling, with the Improved Delayed Detached Eddy Simulation (IDDES) and Reynold-averaged Navier-Stokes (RANS) equations. The project will also only focus on FSI coupling at a single cavity surface as a more detailed simulation was deemed too costly. Simulation resources are provided by the National Academic Infrastructure for Supercomputing in Sweden (NAISS) at Swedish User and Project Repository (SUPR) [15] , under course requirements, and therefore an optimal mesh will be unachievable. This will lead to suboptimal results, which will be discussed and considered accordingly.

2
Theory

Fundamentals of fluid dynamics necessary for the project will be introduced first. The relevant FSI theory will establish the fluid domains' interaction with the solid structure through the flow. Finally, aero-vibro acoustics will cover the induced sounds and vibration in the structure that causes the sound to propagate.

2.1 Fundamentals of Fluid dynamics

The fluid velocity and pressure fields are calculated using the Navier-Stokes equations seen in [16]. The equations are solved using algorithms that iterate over the domain given initial boundary conditions (BC). The project handles a turbulent flow regime, this implies that the flow is divided into two components, mean flow velocity, denoted by $\overline{v}$, and a fluctuating velocity, denoted by v'. It is a common convention, when observing the flow, to take into account the mean flow properties. It is therefore possible to express the velocity as $v = \overline{v} + v'$, applying it to the Navier-Stokes equations and averaging over time achieving what is commonly known as the Reynolds-averaged Navier-Stokes (RANS) and equation given as:

$$\begin{aligned}\frac{\partial \overline{u_i' u_j'}}{\partial t} + \bar{u}_k \frac{\partial \overline{u_i' u_j'}}{\partial x_k} = &- \overline{u_i' u_k'} \frac{\partial \bar{u}_j}{\partial x_k} - \overline{u_j' u_k'} \frac{\partial \bar{u}_i}{\partial x_k} + \overline{\frac{p'}{\rho}\left(\frac{\partial u_i'}{\partial x_j} + \frac{\partial u_j'}{\partial x_i}\right)} \\ &- \frac{\partial}{\partial x_k}\left(\overline{u_i' u_j' u_k'} + \frac{\overline{p' u_i'}}{\rho}\delta_{jk} + \frac{\overline{p' u_j'}}{\rho}\delta_{ik} - \nu \frac{\partial \overline{u_i' u_j'}}{\partial x_k}\right) \\ &- 2\nu \overline{\frac{\partial u_i'}{\partial x_k}\frac{\partial u_j'}{\partial x_k}}.\end{aligned} \tag{2.1}$$

In eq. 2.1 the turbulence kinetic energy can be trace from the term $\overline{v_i' v_j'}$. This resulting RANS equations have more unknowns than the number of the equations which in turn indicates that parts of this equation needs to be modelled. This modelling is referred to as turbulence modelling and as mentioned previously this project will focus on using the Sparlart-Allmaras (SA) model. This model only requires to solve one single equation, a transport equation for a viscosity-like variable $\tilde{\nu}$. The turbulent eddy viscosity and rotation tensor can then be clearly defined, as seen in the works of Spalart and Allmaras [17]. It is to be considered that the SA model usually requires a low wall adjacent cell height, $y^+ < 1$, but this is circumvented by using a wall function giving the possibility to increase the wall adjacent cell height to $30 < y^+ < 100$ thereby reducing the mesh and in turn computational power. It

is therefore seen fit to use SA model with wall functions for this project.

LES is a mathematical model that reduces the complexity of solving all the Navier-Stokes equations, by ignoring to solve small length scales. Doing this reduces complexity and computational costs. This is however still computationally heavy, and therefore combining RANS and LES to what is known as hybrid RANS-LES simulations keeps somewhat of a high resolution while maintaining accurate results. This project uses two different approaches. The first approach is a pure URANS simulation and the second approach is the Improved Delayed Detached Eddy Simulations (IDDES) , a variation of Detached Eddy Simulations (DES) , within hybrid RANS-LES simulations. IDDES is a method suitable for high Reynolds flows. In order to smoothly transition from RANS to LES blending functions must be used, which allows LES to be used away from walls and RANS near walls.

2.2 Fluid-Structure interactions

Fluid-structure interaction is a problem in which fluids and solids interact and influence each other, meaning a combination of computational fluid dynamics (CFD) and computational solid mechanics (CSM) is needed. This type of interaction can have different applications such as water and a boat, bridges starting oscillating due to wind or flutter in airfoils [18]. These types of problems are multi physics problems which usually require either detailed experiments or complex numerical calculations to solve. In numerical calculations, two different approaches can be used: monolithic or partitioned.

The monolithic approach is more expensive in regards to computational power but is also seen as more robust than the partitioned approach. This is because the fluid and solid problem is treated as one combining the equations and solving them altogether. Solving the equations together also means that their influence on each other will be directly taken in to account [18, 19]. A visualization of the monolithic approach can be seen below in Figure 2.1.

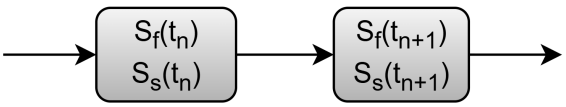

Figure 2.1: Visualization of the monolithic approach.

The partitioned approach means that the fluid equations and the solid equations are solved separately. Individually solving the equations suggests that when the fluid flow is solved the solid domain is not impacted and when the solid domain is solved the flow does not change. The solver computes one of the equations using the computed properties as a boundary condition to solve the other equation. For this exchange of information to occur a face coupling is made. Depending on the type of coupling that is made the information exchanged differs, this could be a one or a two way coupling [18, 19]. A visualization of the partitioned approach can be

seen below in Figure 2.2.

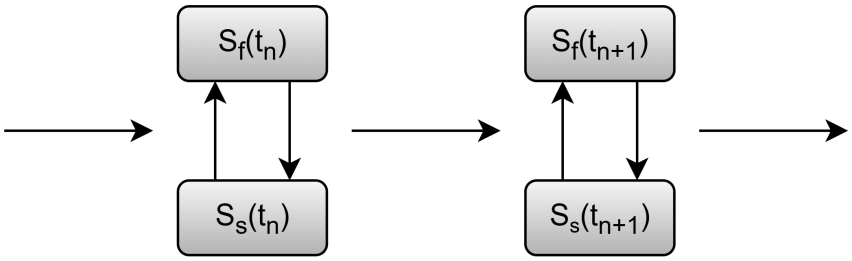

Figure 2.2: Visualization of the partitioned approach.

One-way coupling is used when one of the components, for example, the fluid flow, changes the form or position of the solid structure but the change in the fluid flow caused by the change of the solid structure is negligible. It could also be the other way around that a structural movement affects the flow but the flow changes the structure negligibly, which means a one-way coupling could be used. The solver for when the fluid flow is affecting a solid structure but not the other way around functions as follows: First the fluid model is computed until convergence, then the result is applied to the structural model. For example, interpolating the pressure from the fluid to the surface of the structure, finally, the solid equation is solved and then a new time step is taken starting the loop over. This scheme is visualized in Figure 2.3 [18, 19].

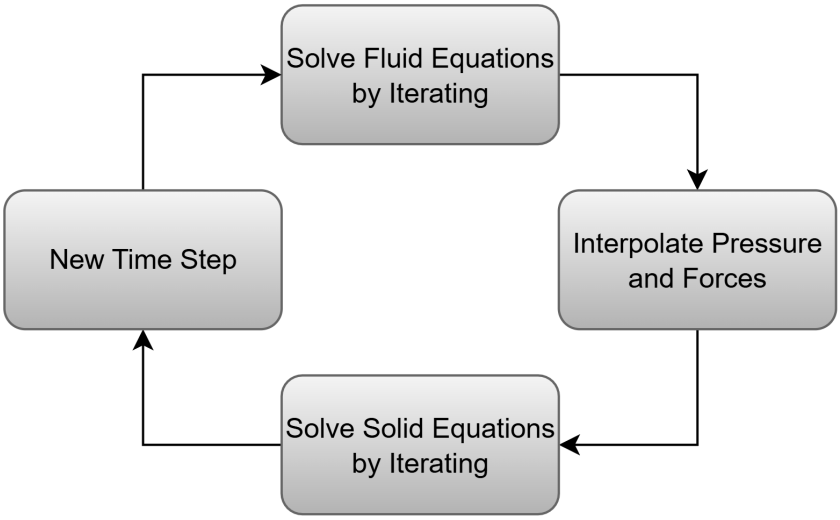

Figure 2.3: Visualization of solver with one-way coupling.

Apart from one-way coupling, there is also two-way coupling. The two-way coupling is used when neither of the individual effects is negligible meaning that a fluid flow affects the structure, which for example deforms, and due to that deformation the fluid flow changes. This method begins by solving the fluid flow, then transfers the solved pressure fields asserting it on the solids surface and is therefore used as a

boundary condition for the solid deformation to occur. As the solid deforms, so will the fluid in return. This process will then repeat and cause oscillations and a two-way coupled FSI system [18]. A visualization of the algorithm is shown in Figure 2.4.

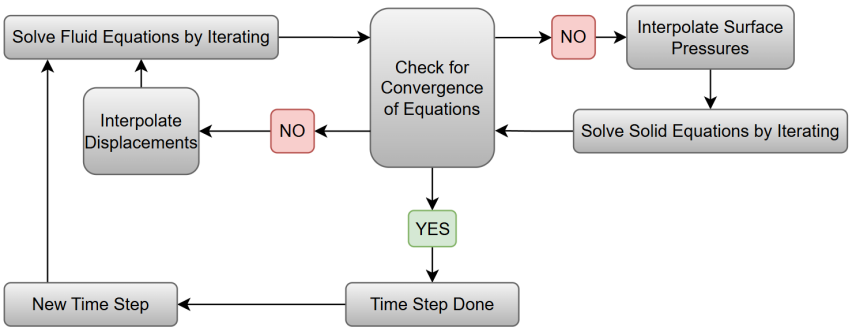

Figure 2.4: Visualization of solver with two-way coupling.

2.3 Aero-vibro Acoustics

Aero-vibro acoustics is a multidisciplinary field that combines principles of aerodynamics, structural dynamics, and acoustics to study and predict the generation, propagation, and interaction of sound in flowing fluids, particularly in scenarios involving vibrating or flexible structures. This field finds application in various industries, including aerospace, automotive, and environmental engineering, where an understanding of noise generation and control is critical [20].

In fluid flows, there is a potential of the flow inducing noise and it is possible to approximate these noise sources induced by the flow. These noise sources can originate from different things in the flow such as bluff body flow, high-speed turbulent shear flow, vibration in the structure induced by the fluid, or turbulent boundary layer flow. These noises can be approximated with computational aeroacoustics (CAA) and are possible to detect in STAR-CCM+. The noise usually propagates from the near field region created by turbulence, geometrical singularities for instance an edge, or mean flow gradients, or both. The noise created in the near-field can be calculated using LES or DES. Using the high-fidelity solution for the near field noise in combination with a mesh-based CAA solver which is accurate such as Linear Euler Equations (LEE) or Acoustic Perturbation Equations (APE). The near-field noise can also be coupled with the Ffowcs William-Hawking Equation (FW-H) to a cost-effective way to approximate the far-field noise. The model is based of Farassat's Formulation 1A and the Dunn Farassat Padula Formulation 1A. [20].

The sound waves in the fluid will cause a local change in pressure. This local pressure change about the ambient pressure is the sound pressure. The sound pressure can be measured at a logarithmic scale of the effective sound pressure to a reference pressure. This measure is in unit dB and is called sound pressure level (SPL). This

is calculated as:

$$SPL = 20log_{10}\left(\frac{p_{rms}}{p_{ref}}\right). \tag{2.2}$$

In eq. 2.2, p_{rms} is the pressures root mean square and the p_{ref} is the reference pressure which is usually 20 μPa [20]. So to get the Overall Sound Pressure Level (OASPL) over all frequencies that has been picked up by the microphones the following formula is used with the same reference pressure:

$$OSPL = 10log_{10}\left(\frac{\sum_i (p^2_{rms})_i}{p_{ref}}\right). \tag{2.3}$$

3
Methods

3.1 Model Setup and Mesh

When setting up the fluid it was desired to replicate the wind tunnel tests [5]. The measurements for the geometry and computational domain were based on previous studies [5]. In Figure 3.1 this CAD model can be seen. Then a fluid domain around this piece was created with measurements given by S. Nilsson et al [5] . The domain can be seen in Figure 3.1. The boundary conditions were set inlets and outlets at the front and back of the domain with no-slip walls around the model to simulate a wind tunnel setting.

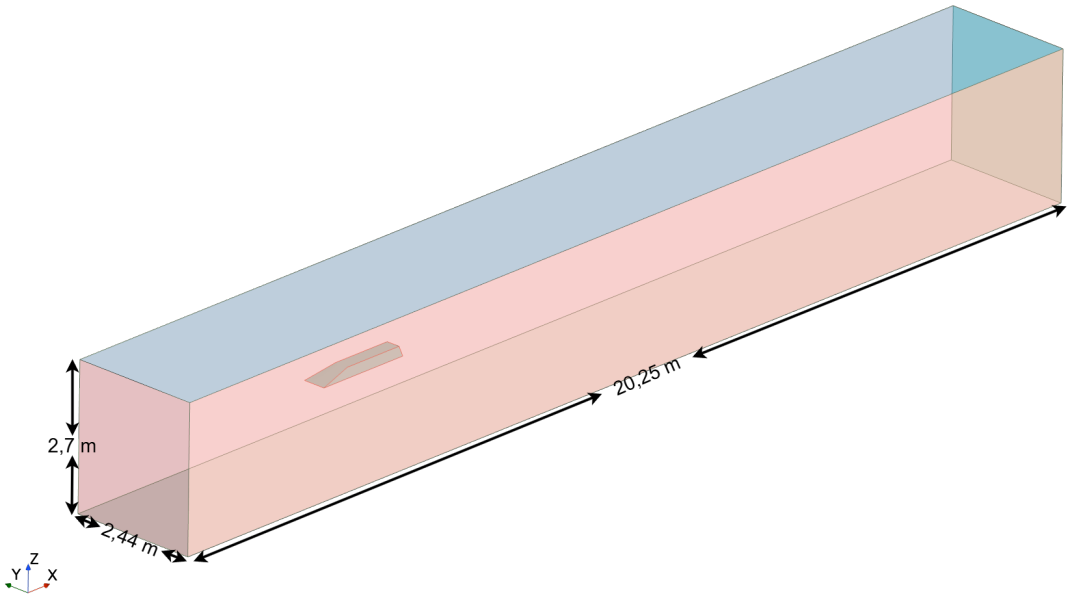

Figure 3.1: Computational domain illustrated with measurments.

When the domain had been assembled, the next step was to generate the volume mesh. The volume mesh was created using an unstructured trimmed cell mesher with prism layers generated near walls.

Taking into consideration what type of turbulence model was used to solve the problem. For this case the SA modeling was used together with a wall function meaning that the wall adjacent cell size was desired to be in the range of $30 < y^+ < 100$. To simplify the meshing process this constraint on the wall adjacent cells was kept mainly for the surface on which the cavity was placed. This resulted in a cell height below 30 in some regions. For a clarification regarding at what y^+ distance the first cell is over the entire part see Figure 3.2 below.

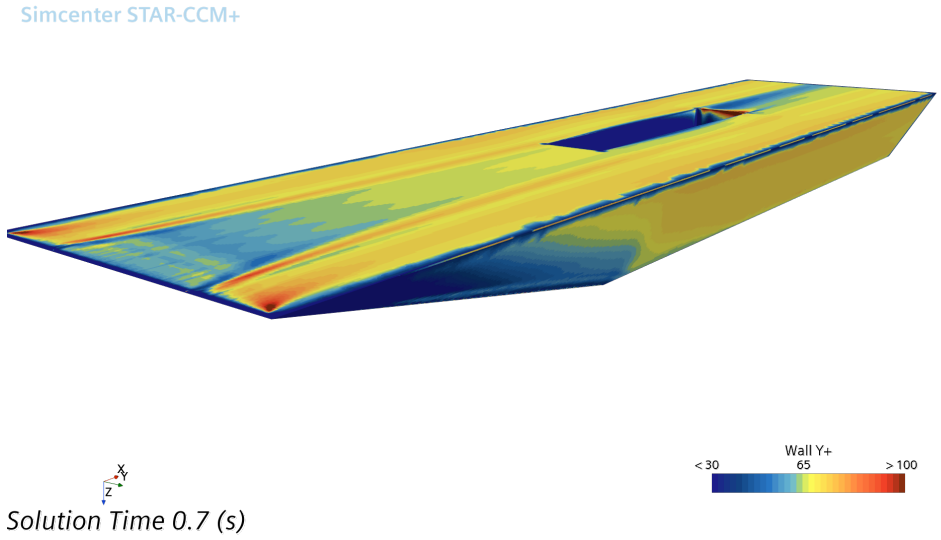

Figure 3.2: y^+ over the submerged body.

To get a initial guess of the desired cell height an online calculator for y^+ was used and then a simulation was made to be able to get the actual cell heights in y^+ over the domain. After the simulation the mesh was refined or coarsened depending on whether the y^+ was to high or to low. The simulation was then done again and the mesh adjusted as needed until satisfactory result was given. The mesh also included a refinement at the top of the cavity to be able to capture the vorticies at this region better. The final mesh was set with a target mesh size equal to 20 mm with 12 prism layers and a total prism layer thickness of 5.5 mm. The cavity refinement ended up with the target size set to 4 mm together with a 2 mm target size at the trailing and leading edge to capture the gradients better. The leading edge mesh can be seen down below in Figure 4.5 The mesh contains a total of 6.22 million cells. The mesh was created using best practices for the chosen turbulence model and aero-acoustic demands [20].

3.2 Fluid Setup

When the domain had been meshed the next step was to setup the simulation parameters. The flow was modeled using a gas with an ideal gas assumption with a viscous regime that is considered to have turbulent flow conditions. For the turbulence model, the Spalart-Allmaras Turbulence Model was used. In addition, the “Solution Interpolation” and “Cell Quality Remediation” models were integrated to ensure nu-

merical stability and accuracy. The standard Ffowcs Williams-Hawkings (Unsteady) model was used for aeroacoustic investigations for the far field, which allows an effective analysis of sound propagation in unsteady fluid flows. This setup should enable a detailed investigation of the relevant acoustic phenomena. An overview of the simulation setup can be seen in Table 3.1.

A precursor simulation was run in a quasi-steady state without morphing and coupling to develop a flow field and increase stability. Once the quasi-steady solution was converged the time-step was lowered and the coupling was activated.

Group Box	**Model**
Fluid Type	Air
Equation of State	Ideal Gas
Flow Type	Coupled Flow
Viscous Regime	Turbulent
Turbulence Model	Reynolds-Averaged Turbulence
Turbulence Closure Model	Spalart-Allmaras Turbulence Model
Aeroacoustics Model	Ffowcs Williams-Hawkings Unsteady
Additional Models	Solution Interpolation
	Cell Quality Remediation
	On-the-Fly FW-H

Table 3.1: Simulation Setup for the Airflow around the Cavity.

The gas parameters for air stored in STAR-CCM+ is presented in Table 3.2 below:

Property	**Value**
Dynamic Viscosity (μ)	1.85508×10^{-5} Pa·s
Molecular Weight (M)	28.9664 kg/kmol
Specific Heat (c_p)	1003.62 J/kg·K
Thermal Conductivity (k)	0.0260305 W/m·K
Turbulent Prandtl Number (Pr_t)	0.9

Table 3.2: Material Properties of Air.

3.3 Solid Setup

There were two main options to choose when it came to the solids deformations. The first one was to do the CSM in STAR-CCM+ and the second one would be to couple STAR-CCM+ with Abaqus and do the CSM in Abaqus. The Abaqus software is especially good for cases of large deformations [21], but the assumptions for the plate in this case is that the deformations will be small meaning engineering strains should be accurate enough. With this in mind the decision was made to do all of

the simulations in STAR-CCM+. The geometric data and material parameters were adopted from Nilsson et al. [5]. The material for the solid is aluminium. STAR-CCM+ has a material database which contains the material properties of different materials. The material properties used for aluminium can be seen below in Table 3.3.

Density [kg/m^3]	**Young's Modulus** [GPa]	**Poisson's Ratio**
2700	70	0.33

Table 3.3: Material properties for aluminium

No damping effects were included in the simulation. The solid material behavior was modeled using isotropic linear elasticity with linear strains without incorporating plasticity and elasticity. Body loads were also neglected.

Small displacements within the structure is assumed in relation to the initial size of the structure. Consequently, the solid setup was not performed in Abaqus. Instead, STAR-CCM+ was employed to configure the fluid, solid, and FSI simulations.

3.3.1 Mesh

In this FSI coupling case, the focus is on the structural vibrations of the cavity bottom. The structural domain was coupled with the fluid (air) solely at the cavity bottom to optimize computational efficiency and reduce system complexity. This simplification allowed for a reduced structural model, represented by the cuboid shown in the figure. The cuboid dimensions correspond to the area of the cavity bottom, extruded by $\pm 3\,\text{mm}$ along the z-axis (relative to the figure's coordinate system). The final finite element (FE) model comprises 21025 elements, discretized using a quadrilateral mesh. The mesh can be observed in Figure 4.6.

3.3.2 Natural frequency

For the plate a brief analysis of the natural frequencies was conducted in Abaqus. The plate was modeled as a 3D shell with a length of 508 mm (20 inches), width of 101.6 mm (4 inches), and a thickness of 3 mm. The section was set around the mid plane and the material parameters was set after the material parameters for aluminum from STAR-CCM+ which can be seen in Table 3.3 Since the frequency calculation was relatively cheap to do in comparison to the fluid a fine mesh of a quad-elements of a size 0.1 mm was set. The edges was of the plate was pinned so that it could rotate freely but it could not translate in any direction. The job was thereafter submitted.

3.4 Fluid-Structure-Interaction Setup

For the FSI coupling, the "Mapped Contact Boundary" method was employed. The FSI coupling specification was defined as "Fluid Load - Pressure & Wall Shear

Stress", enabling the transfer of pressure and wall shear stresses as loads onto the structure. "Solid Displacement" was selected as the motion specification for the solid region. This setting allows the structural mesh to deform in real-time based on the computed displacements. In the fluid region, morphing was chosen as the motion specification, enabling the fluid mesh to adapt according to the displacements mapped onto the interface between the fluid and the structure.

Boundary conditions were applied by fixing the outer walls of the solid segment, thereby constraining their motion. (This approach was chosen because the primary focus is on the structural vibrations of the plate, particularly on the vertical displacement within the plate's interior.)

3.5 Aeroacoustics

To catch the noise created by the flow and the structure, microphones were positioned out in the domain. Three microphones were placed inside the cavity at the front, middle and back of the bottom of the cavity. Then, there were five microphones placed in the free stream. These five microphones were placed with one at the leading edge, one at the trailing edge, one right below the middle of the cavity and one at ± 45 deg from the free stream microphone centered to the cavity. For a clarification of the microphone placements see Figure 3.3 where the red circles, ●, denote the far field free stream microphones and the yellow circles, ●, denote the microphones placed on the surface of the plate. Furthermore, the figure illustrates the mesh frequency cutoff. This was analyzed to gather an understanding of what frequencies were captured in the different regions.

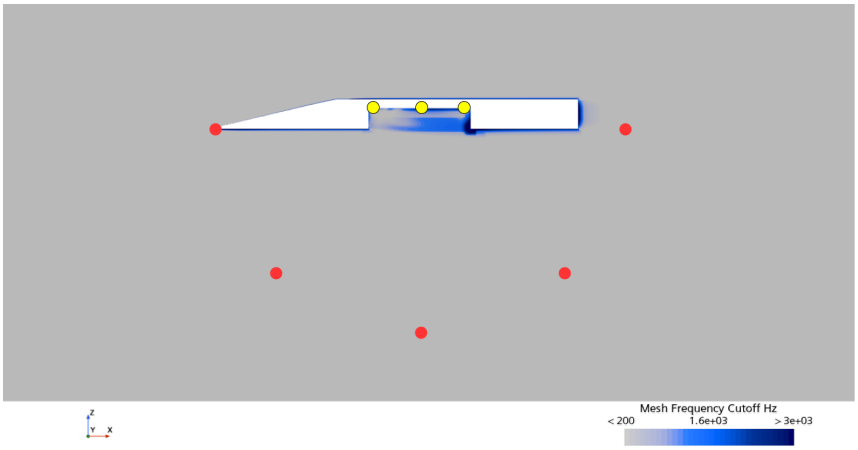

Figure 3.3: Microphone placements and Mesh Frequency Cutoff.

4

Results

During this chapter the result from the different parts will be covered. First is how the mesh turned out, both for the fluid and for the solid followed by the results given from the flow solved by the two different models.

4.1 Mesh

A front view of the mesh for the domain can be seen in Figure 4.1 and a side view of the mesh for the domain can be seen in Figure 4.2. The element size is color coded in the side view plot to give a clearer view of the sizes of the elements in different areas.

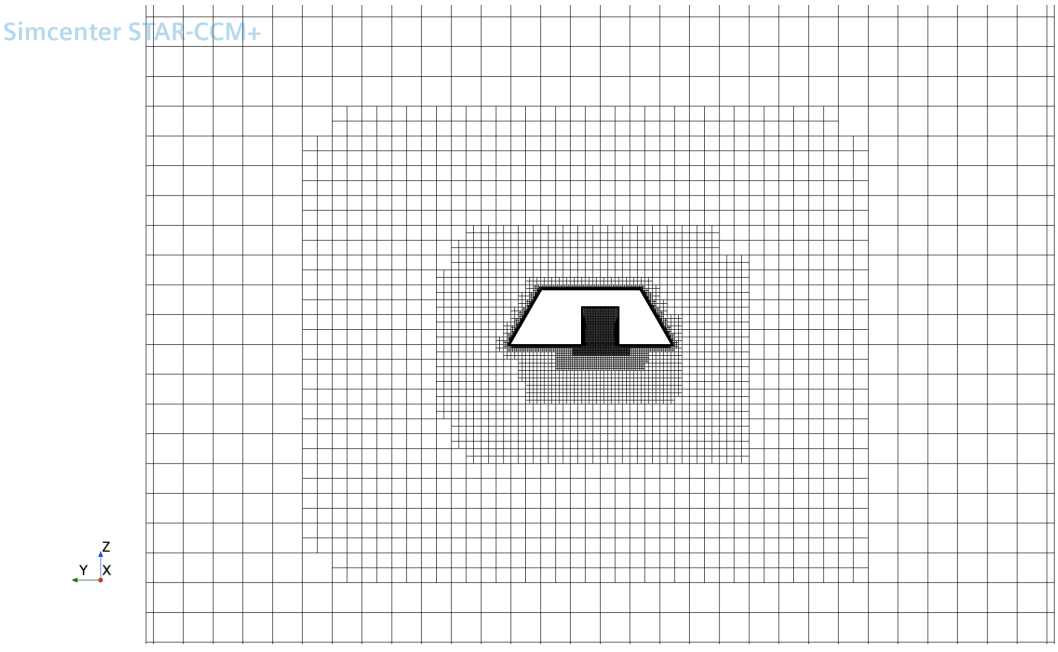

Figure 4.1: Volume mesh as seen from the front.

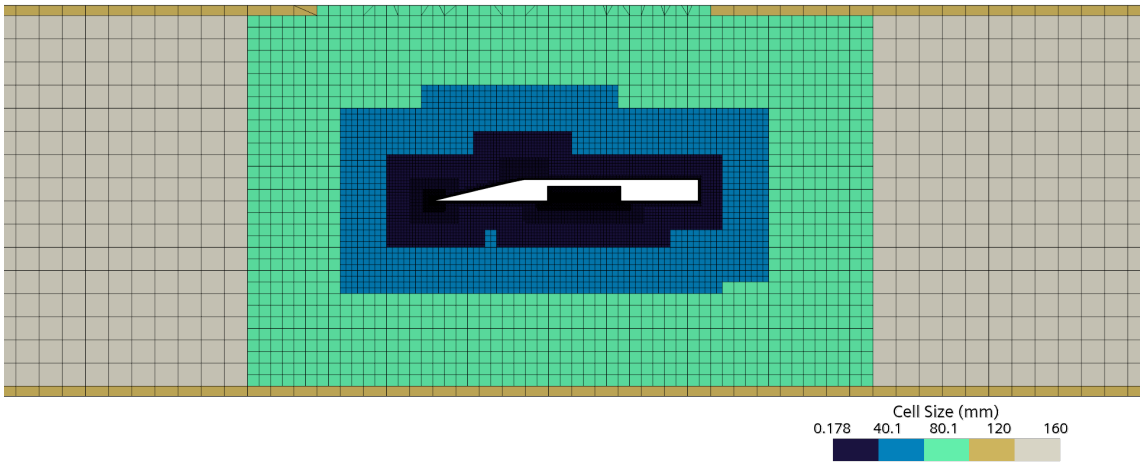

Figure 4.2: Distribution of Mesh Sizes as seen from the side.

A close up on the cavity mesh can be seen in Figure 4.3 and a close up of the mesh of front corner of the cavity can be seen in Figure 4.4

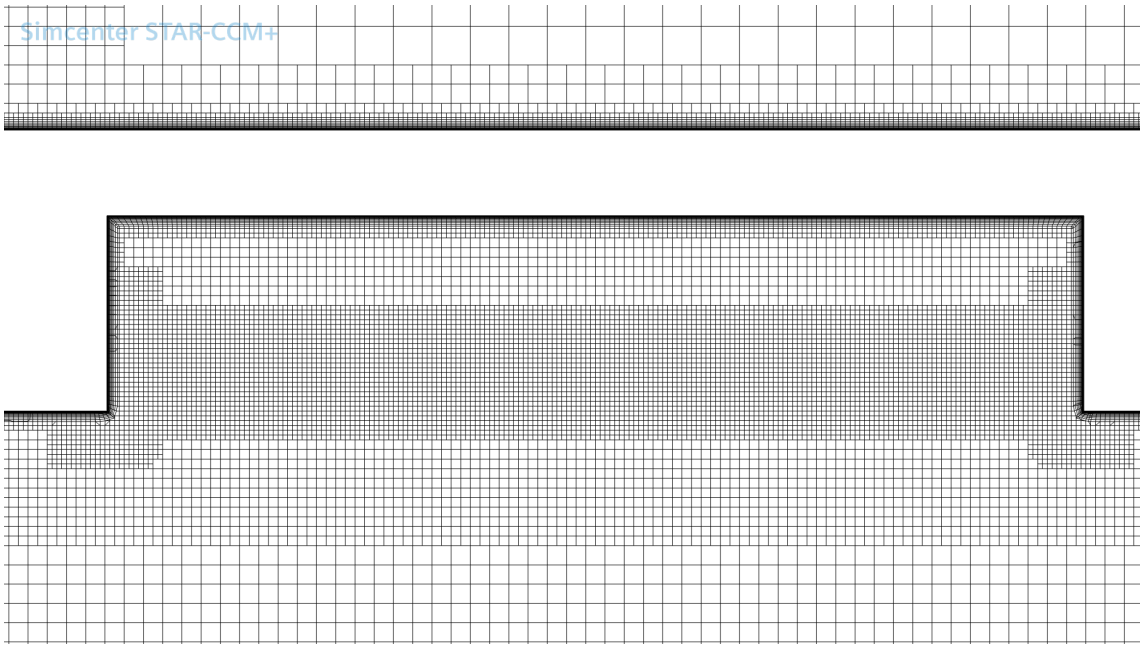

Figure 4.3: The mesh as seen with a focus of the cavity.

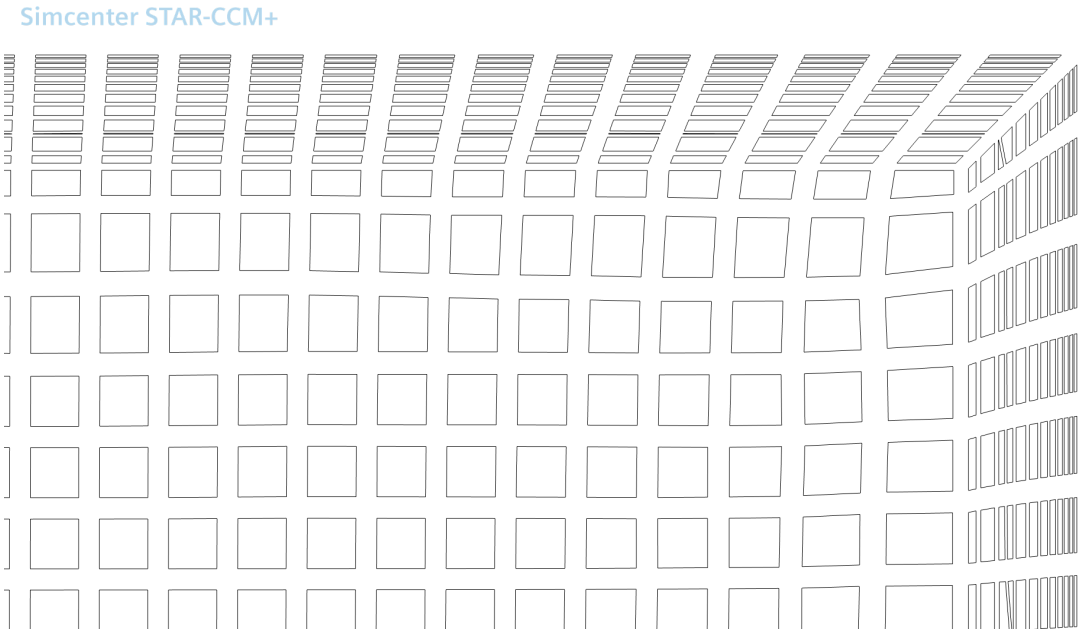

Figure 4.4: Mesh as seen from the front with a focus on the corner of the cavity.

Mesh at leading edge in Figure 4.5

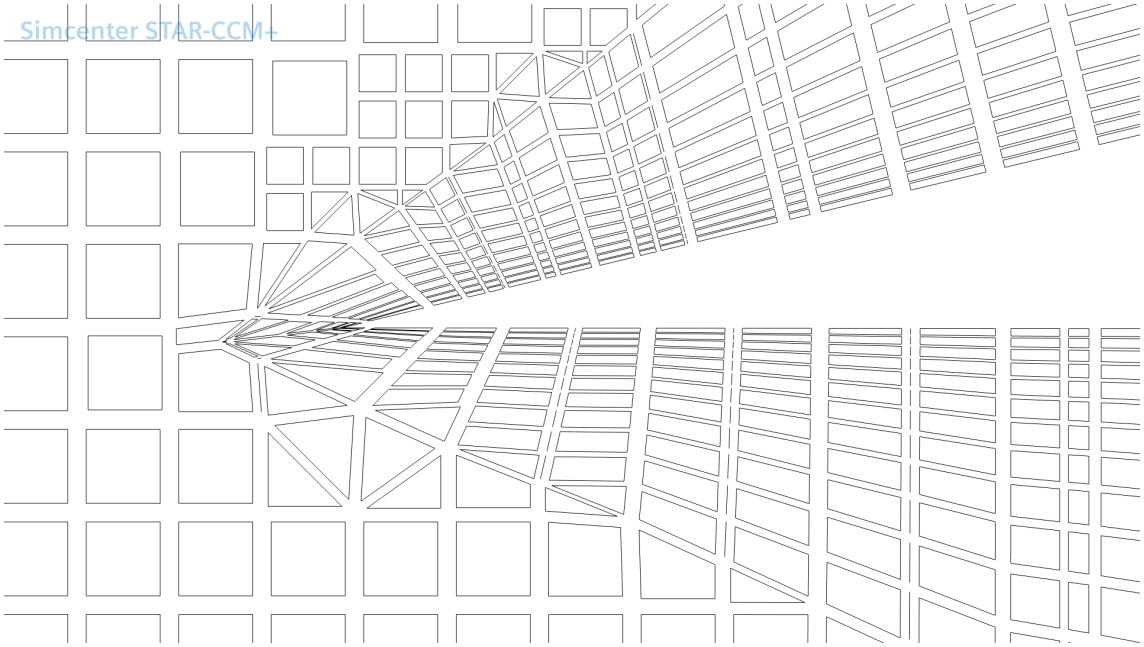

Figure 4.5: Mesh at the leading edge.

Looking at the interface between solid and fluid, there is a total of 4200 elements and the mesh of the solid can be seen in Figure 4.6

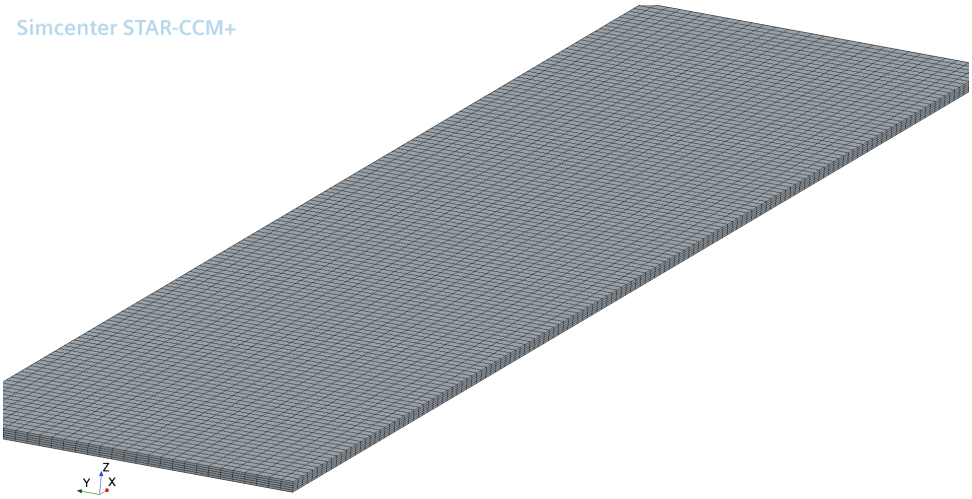

Figure 4.6: FEM mesh of the solid body.

4.2 The URANS approach

Unsteady-RANS (URANS) builds on the RANS methodology by expanding it to include time-dependant terms. The results discovered for this simulation method will be discussed in this section.

4.2.1 Fluid domain results

Pressure field and relative Mach Number can be observed in Figures 4.7 and 4.8. The figures illustrate increased pressure and velocity on the wedge with Mach waves propagating from the geometry, creating a pressure wave and increased sound. Furthermore, the figures illustrate a higher pressure on the top of the geometry compared to the bottom. This indicates that the flow-based sound is caused more by the geometry surrounding the cavity compared to the vibration of the plate, on the top of the body.

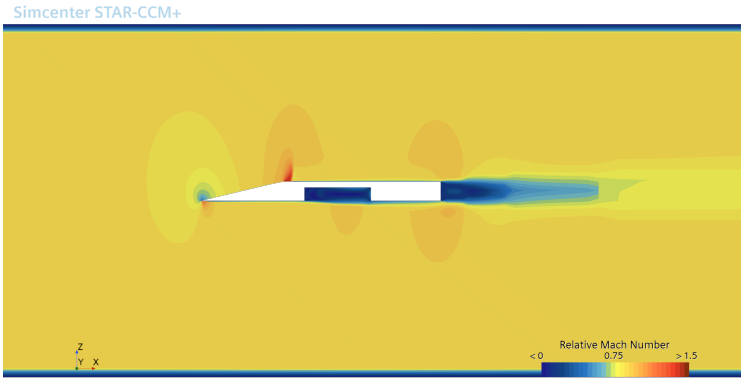

Figure 4.7: Relative Mach Number as seen from the side.

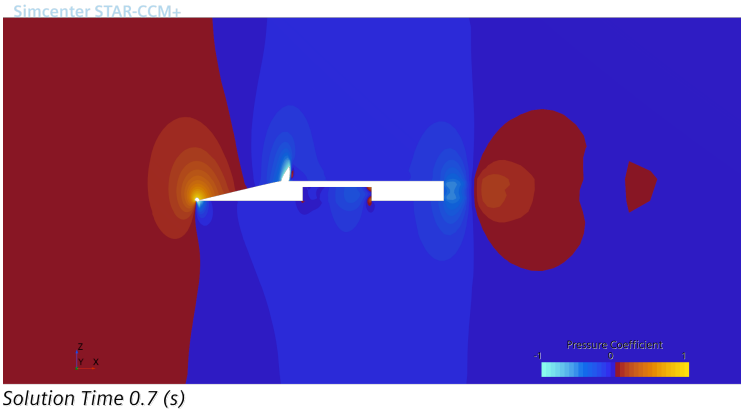

Figure 4.8: Pressure Coefficient distribution as seen from the side.

4.2.2 Solid domain

Observing the result from the natural frequency analysis of the aluminum plate a total of 7 natural frequencies could be found in between the span of 2500 Hz. The frequencies are presented in Table 4.1.

Natural Frequency	$\mathbf{f_1}$	$\mathbf{f_2}$	$\mathbf{f_3}$	$\mathbf{f_4}$	$\mathbf{f_5}$	$\mathbf{f_6}$	$\mathbf{f_7}$
Value	738	820	959	1154	1406	1715	2080

Table 4.1: Natural Frequencies of Aluminium Plate.

The deformation caused by the flow that was calculated in STAR-CCM+ is illustrated in Figures 4.9 and 4.10. The results show a large deformation at the front with a smaller deformation at the back of the cavity with a symmetric behavior.

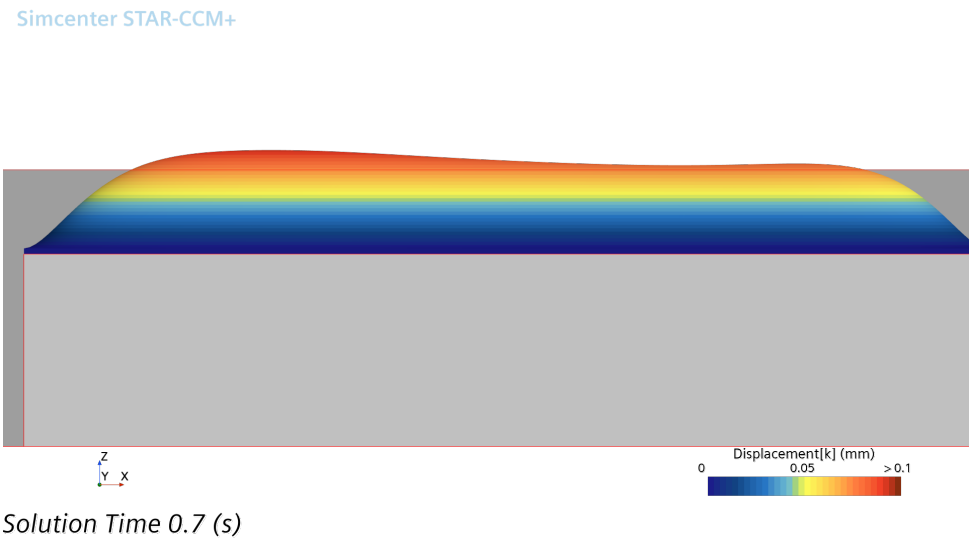

Figure 4.9: Deformation of the plate at the end of the simulation, scaled.

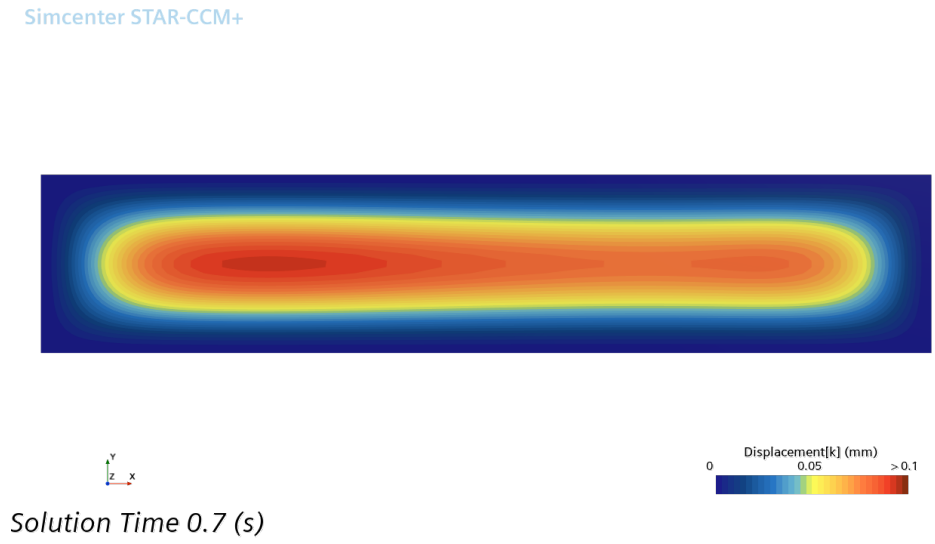

Figure 4.10: Displacement of the plate at the end of the simulation, unscaled.

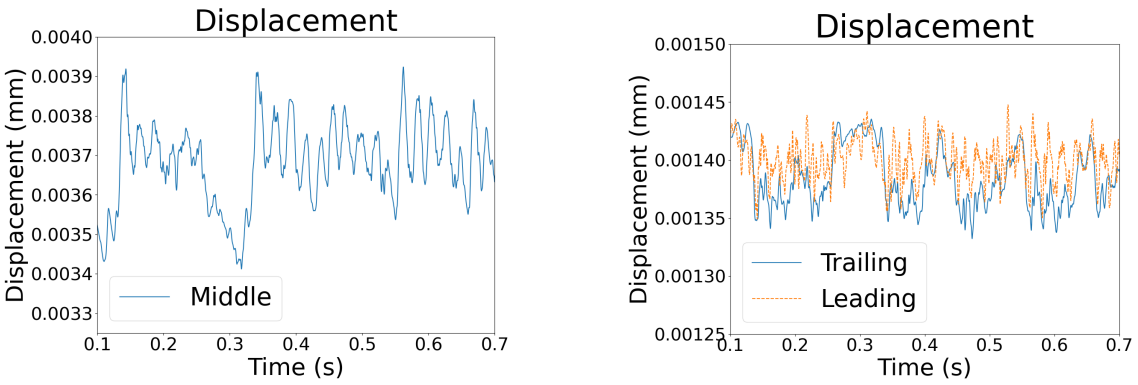

(a) Middle node.

(b) Leading and trailing edge.

Figure 4.11: Displacement versus time at the different receivers.

4.2.3 Aeroacoustic

The different microphones placed over the domain picked up different sound pressure levels. The result from the microphones placed inside the cavity can be seen in Figure 4.12 and the sound picked up by the microphone in the far field picked up the SPLs presented in Figure 4.13. The vertical lines seen in both figures is the natural frequencies of the bottom plate of the cavity which have been presented in Table 4.1.

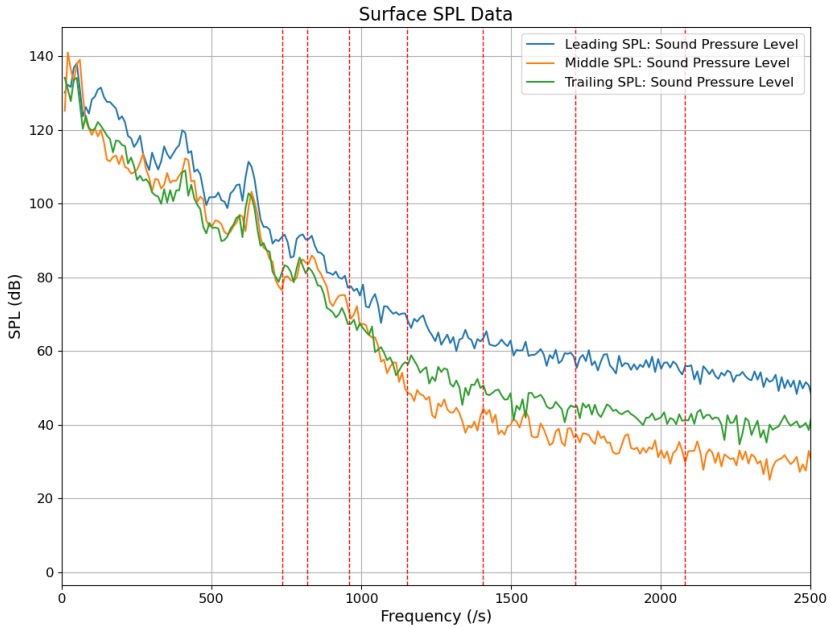

Figure 4.12: SPL picked up by microphones inside the cavity for the URANS model

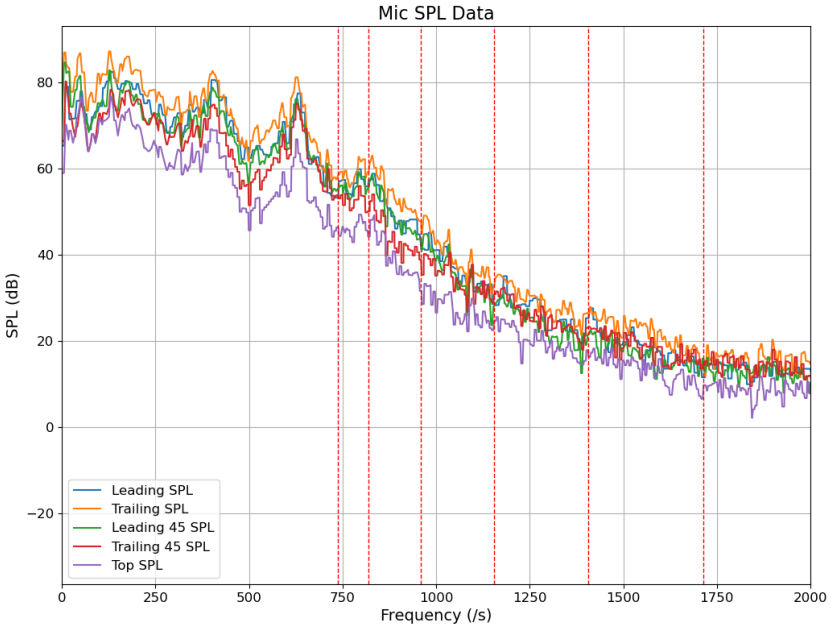

Figure 4.13: SPL picked up by microphones in the free stream for the URANS model

The overall sound pressure level (OASPL) can be observed in Table 4.2. An increased OASPL can be observed at the surface-mounted receivers compared to the far field receivers. We can also observe a difference in the OASPL between the receivers mounted at the leading at trailing edge in the far field and the ones mounted directly below the plate.

Measurement Point	**Sound Pressure Level (dB)**	**Location**
Leading	154.22	Surface Mounted
Middle	155.57	Surface Mounted
Trailing	150.64	Surface Mounted
Leading	102.88	Far Field
Top	95.68	Far Field
Trailing	107.74	Far Field
Leading 45	103.56	Far Field
Trailing 45	99.78	Far Field

Table 4.2: OASPL for Different Measurement Points.

4.3 The IDDES approach

The corresponding IDDES simulations are executed, and the results are presented in the coming section. The intent is to observe the differences in simulation methods and to contribute to an extensive discussion further in the report.

4.3.1 Fluid domain results

The pressure distribution and relative Mach Number can be observed in Figures 4.14 and 4.15. The figures illustrate a wake of higher detail with a big high pressure done close to the top half. We can also see high-pressure areas above the vibrating plating, indicating an effect from the FSI.

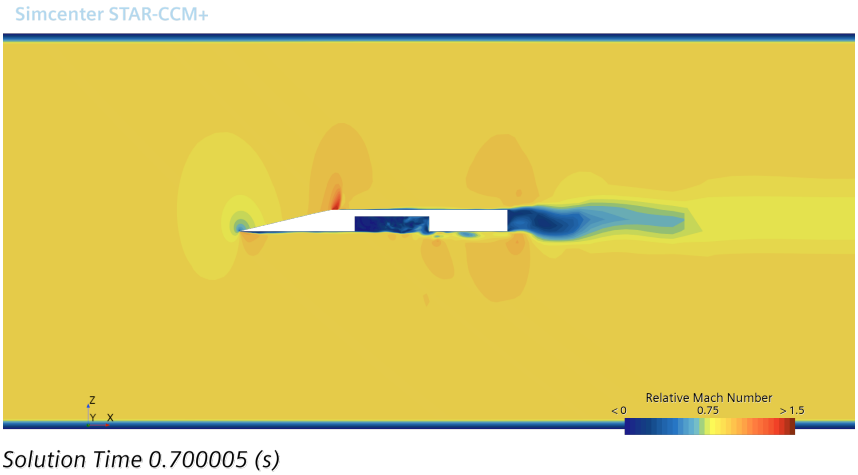

Figure 4.14: Relative Mach Number as seen from the side.

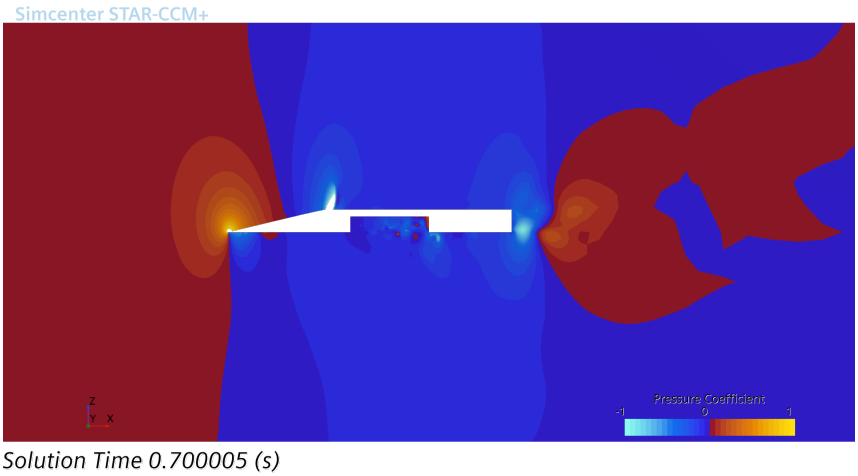

Figure 4.15: Pressure Coefficient distribution as seen from the side.

4.3.2 Solid domain

The solid has the same eigen frequencies as with the URANS approach as the solid is uncheached. Observing Figure 4.16 we can see big deformations close to the leading and trailing edges of the plate with a symmetric behaviour as illustrated in Figure 4.17.

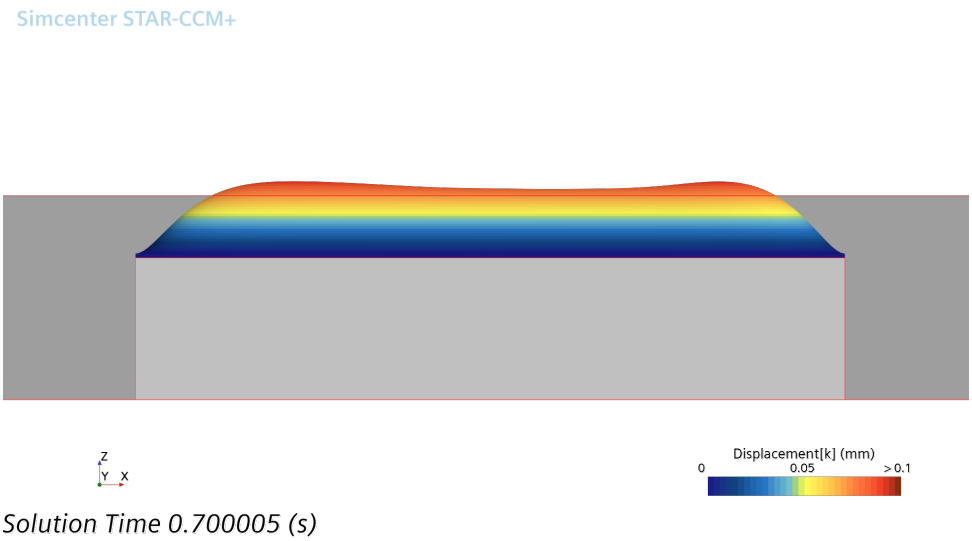

Figure 4.16: Deformation of the plate at the end of the simulation, scaled.

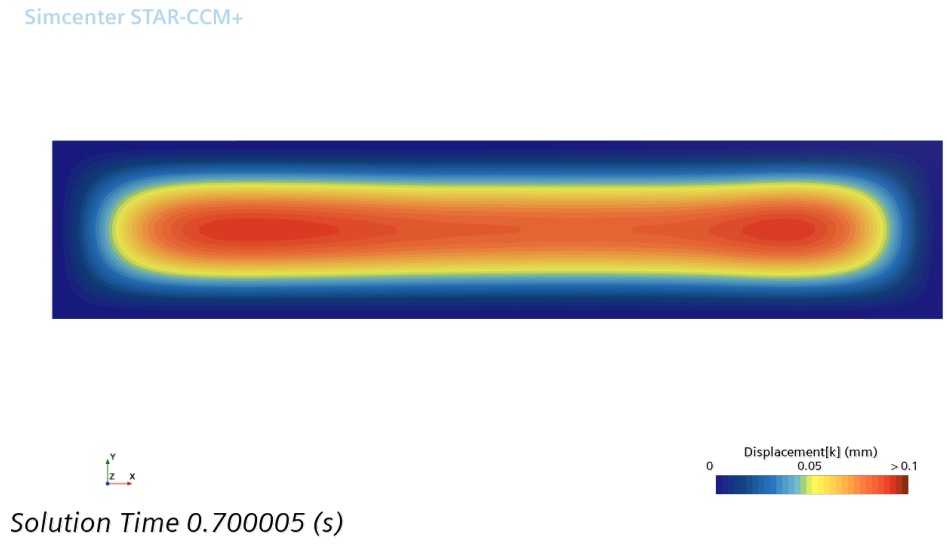

Figure 4.17: Displacement of the plate at the end of the simulation, unscaled.

The displacement against time can be observed in Figure 4.18.

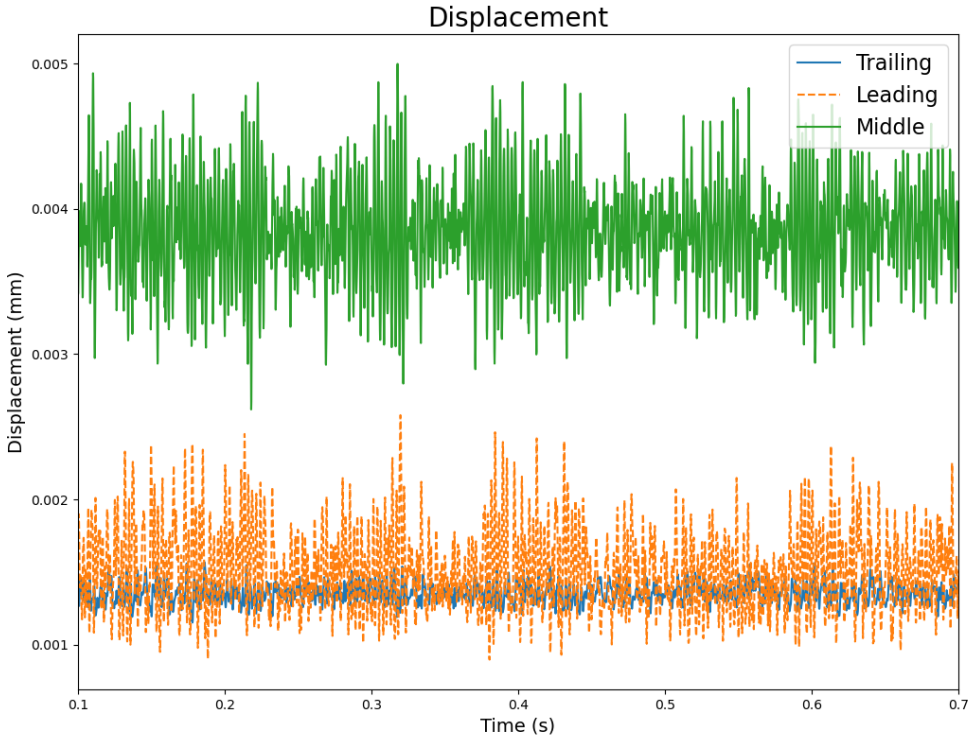

Figure 4.18: Displacement versus time at the different receivers.

4.3.3 Aeroacoustics

The result from the microphones placed inside the cavity can be seen in Figure 4.19 and the sound picked up by the microphone in the far field picked up the SPLs presented in Figure 4.20. The vertical lines seen in both figures is the natural frequencies of the bottom plate of the cavity which have been presented in Table 4.1.

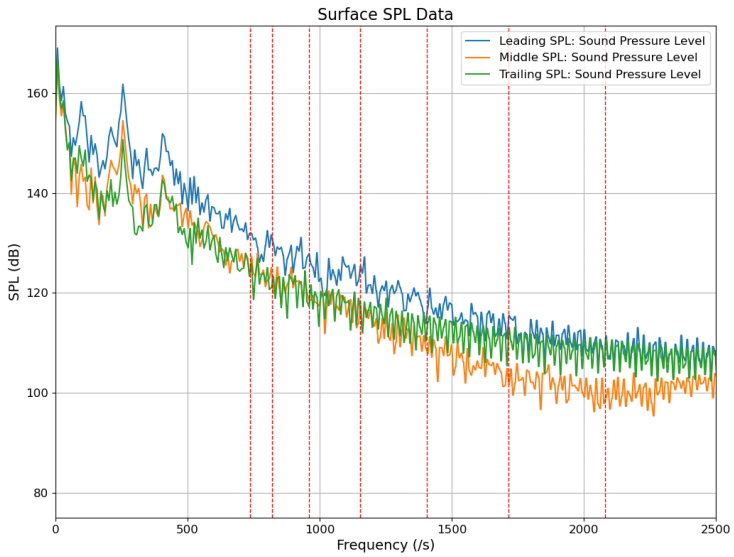

Figure 4.19: SPL picked up by microphones inside the cavity for the IDDES model

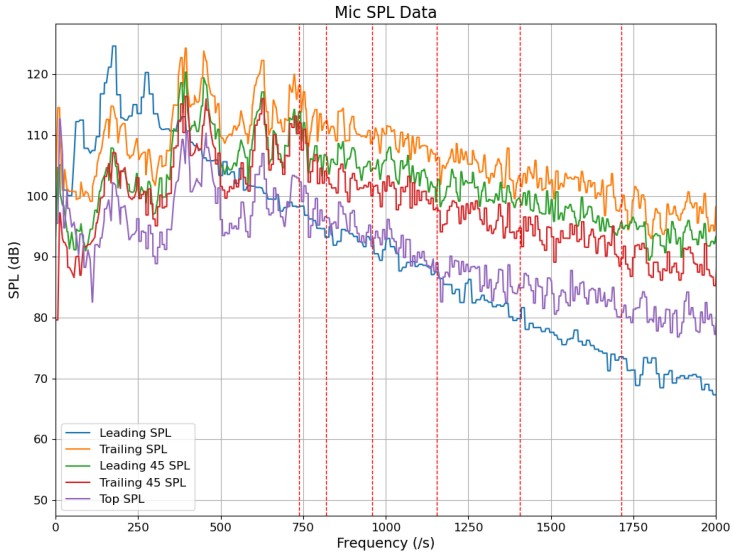

Figure 4.20: SPL picked up by microphones in the free stream for the IDDES model

The OASPL for the IDDES results can be observed in Table 4.3. Also here an increased OASPL can be observed at the surface-mounted receivers compared to the far field receivers. A difference in the OASPL can be observed between the receivers mounted at the leading at trailing edge in the far field and the ones mounted directly below the plate.

Measurement Point	**Sound Pressure Level (dB)**	**Location**
Leading	182.00	Surface Mounted
Middle	177.72	Surface Mounted
Trailing	178.39	Surface Mounted
Leading	139.85	Far Field
Top	130.94	Far Field
Trailing	144.63	Far Field
Leading 45	141.61	Far Field
Trailing 45	137.26	Far Field

Table 4.3: OASPL for the IDDES approach.

5
Discussion

Looking at the result for the SPL it can be seen that there are smaller peaks of the SPL at the natural frequencies for the lower natural frequencies of the plate, which is to be expected. Although the highest peaks are seen at frequencies lower than the natural frequencies of the plate. This sound is simply caused by the flow and not the structural vibrations. Compared to the results provided by S. Nilsson et al [5], the frequency span that is captured is not ideal. One major area that is causing this difference is the coarse mesh used in this project. This report investigated the results from two approaches, URANS and IDDES, which will be considered in the coming sections.

5.1 The URANS approach

As expected from a URANS simulation the wake of the subject was relatively stable, and not completely resolved as seen in figure 4.7. In turn, the pressure distribution can be observed to be very even. When it comes to the solid domain deformation is observed but in the leading edge clearly, however, this tapers down towards the trailing edge. It would be expected that a more resolved wake would induce more deformation and a clearer behavior of the solid domain, especially when observing the trailing edge.

Observing the aero-acoustic results it is clear that the simulation is not properly resolving the fluctuations required to capture the higher frequencies, hence the rapid flattening of the curve. The OASPL is significantly larger on the plate compared to in the freestream with the far field receivers having a big decline in percieved SPL.

The displacement shows a periodicity as seen in Figure 4.11 with larger fluctuations in the middle compared to the leading and trailing edges. This indicates that the main vibration induced sound is created from the middle of the plate.

5.2 The IDDES approach

When observing the fluid domain solution in the IDDES model, wake and large-scale turbulence can clearly be seen in Figure 4.14. These fluctuations in pressure distribution were observed to have a high level of impact on the FSI solution. In the solid domain, it is possible to observe a clear deformation towards the trailing edge. One thing to note is the stability of the measured displacement with the IDDES

method.

Observing the results from the aero-acoustic analysis in the freestream it is possible to see a major spike at the lowest eigenfrequency of the plate together with spikes in the 200-700 Hz range. The spikes correlating with the eigenfrequency can be assumed to be caused by the vibrations of the plate while the lower frequency spikes are caused by the mean flow. At the surface a high SPL can be observed at all receivers with a fall of towards the higher frequencies, asymptotically reaching a level of 100 dB. The highest OASPL can be observed at the leading and trailing edge of the plate, indicating sources of high noise. In the freestream the farfield receivers indicate that the highest OASPL can be observed at the trailing point and at the receiver placed 45 degrees ahead of the plate. When observing the displacement of the plate a large deformation can be observed in the front and back of the plate. This indicates that the pressure and flow induced forces are largest at these points. Comparing these deformations to the OASPL the high sound pressure level is explained.

5.3 A comparison of the approaches

As mentioned previously, due to the coarse mesh some drawbacks can be seen in both the approaches. An important consideration when observing aero-acoustics is that the dB could be impacted. Since the SPL is a logarithmic measure of the pressure difference. This pressure difference is localized meaning that if the cell becomes bigger the pressure difference in the entire cell will be lower than if the cell would have the size of the localized pressure point. This means that the p_{rms} will be smaller since the cells at the microphone are coarser, and therefore, it could lower the level of dB that is measured. When observing the differences between the two approaches there is a significant difference in the OASPL and SPL for each of the receivers. Observing the Mic SPL data for the URANS approach it could be seen that the frequency ranges from around 80-90 dB at 0-400 Hz to around 20 dB at 1750-2000 Hz. Whereas for the IDDES approach, the mic SPL data seems to jump a lot in the 0-400Hz range with SPL levels from 90 to 120 dB, reaching at its lowest just under 70 dB at 2000 Hz. Surface SPL values also differ significantly between the approaches, where the URANS values extend from a maximum of 140 dB to a minimum of approximately 30dB, and for the IDDES approach these values range from 160 dB to about 100 dB. It can be deduced that the resolvance of large-scale eddies have significant impact on noise resolution. IDDES approach can catch more noise due to more resolved turbulence. Of course this is also observed by the OASPL given by the respective tables in previous sections. There is also a difference in the pressure and velocity fields leading to a difference in the displacements.

6
Conclusion

Although the mesh was relatively limited in its ability to capture all effects, the results were satisfactory within the scope of the study and this project. It should be noted that limited resources were invested in refining the mesh due to time constraints. Nevertheless, it is expected that the accuracy and quality of the results could be significantly improved with increased computational resources, extended simulation time, and a more carefully optimized mesh design.

This study shows a clear and significant difference in the models used to resolve turbulence when it comes to transonic cavity flows from an FSI standpoint. For future work, it could be interesting to investigate how different turbulence models would solve the problem at hand. So for example trying to solve the problem also with k-ω or the k-ϵ model.

Bibliography

[1] M. Kegerise, E. Spina, S. Garg, and L. Cattafesta, "Mode-switching and nonlinear effects in compressible flow over a cavity," *Physics of Fluids - PHYS FLUIDS*, vol. 16, pp. 678–687, Mar. 2004. DOI: 10.1063/1.1643736.

[2] J. Rossiter, "Wind-tunnel experiments on the flow over rectangular cavities at subsonic and transonic speeds," 1964.

[3] Y. Lin *et al.*, "Investigation of the reynolds number independence of cavity flow in 2d street canyons by wind tunnel experiments and numerical simulations," *Building and Environment*, vol. 201, p. 107 965, 2021, ISSN: 0360-1323. DOI: https://doi.org/10.1016/j.buildenv.2021.107965. [Online]. Available: https://www.sciencedirect.com/science/article/pii/S0360132321003693.

[4] M. Nallasamy and K. K. Prasad, "On cavity flow at high reynolds numbers," *Journal of Fluid Mechanics*, vol. 79, no. 2, pp. 391–414, 1977. DOI: 10.1017/S0022112077000214.

[5] S. Nilsson, H.-D. Yao, A. Karlsson, and S. Arvidson, "Effects of aeroelastic walls on the aeroacoustics in transonic cavity flow," *Aerospace*, vol. 9, no. 11, 2022, ISSN: 2226-4310. DOI: 10.3390/aerospace9110716. [Online]. Available: https://www.mdpi.com/2226-4310/9/11/716.

[6] S.-H. Peng, "Simulation of flow past a rectangular open cavity using des and unsteady rans," vol. 1, Jun. 2006, ISBN: 978-1-62410-028-4. DOI: 10.2514/6.2006-2827.

[7] S. Lawson and G. Barakos, "Review of numerical simulations for high-speed, turbulent cavity flows," *Progress in Aerospace Sciences*, vol. 47, no. 3, pp. 186–216, 2011, ISSN: 0376-0421. DOI: https://doi.org/10.1016/j.paerosci.2010.11.002. [Online]. Available: https://www.sciencedirect.com/science/article/pii/S0376042110000631.

[8] K. Luo and Z. Xiao, "Improved delayed detached-eddy simulation of transonic and supersonic cavity flows," *Notes on Numerical Fluid Mechanics and Multidisciplinary Design*, vol. 130, pp. 163–174, Feb. 2015. DOI: 10.1007/978-3-319-15141-0_13.

[9] S.-H. Peng and S. Leicher, "Des and hybrid rans-les modelling of unsteady pressure oscillations and flow features in a rectangular cavity," in *Advances in Hybrid RANS-LES Modelling: Papers contributed to the 2007 Symposium of Hybrid RANS-LES Methods, Corfu, Greece, 17-18 June 2007*, Springer, 2008, pp. 132–141.

[10] D. Basu and A. Hamed, "Des and hybrid rans/les models for unsteady separated turbulent flow predictions," *43rd AIAA Aerospace Sciences Meeting and Exhibit - Meeting Papers*, Jan. 2005. DOI: 10.2514/6.2005-503.

[11] R. Allen, F. Mendonça, and D. Kirkham, "Rans and des turbulence model predictions of noise on the m219 cavity at m=0.85," *International Journal of Aeroacoustics*, vol. 4, no. 1-2, pp. 135–151, 2005. DOI: 10.1260/1475472053730039. eprint: https://doi.org/10.1260/1475472053730039. [Online]. Available: https://doi.org/10.1260/1475472053730039.

[12] P. Łojek, I. Czajka, A. Gołaś, and K. Suder-Dębska, "Influence of the elastic cavity walls on cavity flow noise," *Vibrations in Physical Systems*, vol. 32, no. 1, 2021.

[13] L. Ruiz-Calavera *et al.*, "Verification and validation data for computational unsteady aerodynamics," RTO-TR-26, Tech. Rep., 2000.

[14] L. Larchevêque, P. Sagaut, T.-H. Lê, and P. Comte, "Large-eddy simulation of a compressible flow in a three-dimensional open cavity at high reynolds number," *Journal of fluid mechanics*, vol. 516, pp. 265–301, 2004.

[15] [Online]. Available: https://www.naiss.se/about-us/.

[16] *Navier-stokes equations*. [Online]. Available: https://www.grc.nasa.gov/www/k-12/airplane/nseqs.html.

[17] P. Spalart and S. Allmaras, "A one-equation turbulence model for aerodynamic flows," in *30th aerospace sciences meeting and exhibit*, 1992, p. 439.

[18] R. Subramania Raja, "Coupled fluid structure interaction analysis on a cylinder exposed to ocean wave loading," 2012. [Online]. Available: https://odr.chalmers.se/items/c615ba66-7974-430b-9a48-0d905b3b13cd.

[19] J. Degroot, K. J. Bathe, and J. Vierendeels, "Performance of a new partitioned procedure versus a monolithic procedure in fluid–structure interaction," 2008. [Online]. Available: chrome-extension://efaidnbmnnnibpcajpcglclefindmkaj/https://web.mit.edu/kjb/www/Principal_Publications/Performance_of_a_New_Partitioned_Procedure_versus_a_Monolithic_Procedure_in_Fluid_Structure_Interaction.pdf.

[20] Siemens Digital Industries Software, *Simcenter star-ccm+ documentation*, Hämtad: 2024-04-16, Siemens Digital Industries Software, 2020. [Online]. Available: https://docs.sw.siemens.com/documentation/external/PL20200805113346338/en-US/userManual/userguide/html/index.html#page/connect%2Fsplash.html.

[21] S. N. Ullah, L. F. Hou, U. Satchithananthan, Z. Chen, and H. Gu, "A 3d ritss approach for total stress and coupled-flow large deformation problems using abaqus," *Computers and Geotechnics*, vol. 99, pp. 203–215, 2018, ISSN: 0266-352X. DOI: https://doi.org/10.1016/j.compgeo.2018.01.018. [Online]. Available: https://www.sciencedirect.com/science/article/pii/S0266352X18300284.